

Frequency Tuning of a Disk Resonator Gyro via Mass Matrix Perturbation

David Schwartz, Dong Joon Kim, Robert T. M'Closkey, *Member IEEE*

Abstract

Electrostatic tuning of the resonant modes in microelectromechanical (MEM) vibratory gyroscopes is often suggested as a means for compensating manufacturing aberrations that produce detuned resonances. In high performance sensors, however, this approach places very stringent requirements on the stability of the bias voltages used for tuning. Furthermore, the bias voltage stability must be maintained over the operating environment, especially with regard to temperature variations. A known solution to this problem is to use mass perturbations of the sensor's resonant structure for resonant mode tuning. This paper presents a new mass perturbation technique that relies only on the sensor's integrated actuators and pick-offs to guide the mass perturbation process. The algorithm is amenable to automation and eliminates the requirement that the modal nodes of the resonator be found directly.

A. INTRODUCTION

High-performance vibratory angular rate sensors rely on the matching of the frequencies of two modes that are highly coupled by a Coriolis acceleration term when the equations of motion are written in a case-fixed coordinate system. Frequency matching exploits the mechanical gain afforded by the sensor dynamics and leads to the best attainable signal-to-noise ratio. In principle, the degenerate dynamics can be attained by designing structures with a high degree of symmetry such as Litton's Hemispherical Resonator Gyroscope (HRG)[1] and the BAE Silicon Vibrating Structure Gyroscope (SiVSG) [2]. The subject of this paper is Boeing's Silicon Disk Resonator Gyroscope (SiDRG) shown in Fig. 1. In this device, electrodes that are embedded in the spaces between the concentric rings are used to drive and sense planar vibrations.

Ideally, in each of these sensors the anchor attaching the resonant structure to the sensor case is a nodal point for the Coriolis coupled modes and the symmetric design guarantees degenerate modal frequencies. This scheme

Manuscript submitted on September 21, 2007. This work was supported by Boeing and NSF grant #0601622.

The authors are with the Mechanical and Aerospace Engineering Department, University of California, Los Angeles, CA 90095 USA.

David Schwartz is a Graduate Student Researcher.

Dong Joon Kim is a Postdoctoral Researcher

Robert T. M'Closkey is Professor and corresponding author (310 825-2909, rtm@obsidian.seas.ucla.edu)

isolates the Coriolis-coupled modes from linear base motion and reduces energy dissipation in the modes, thereby eliminating large contributors to angular rate bias and drift. The HRG is an extreme example of the degree of isolation that can be achieved— quality factors exceeding 6×10^6 have been reported when the resonators are fabricated from fused quartz [1], [3].

For those sensors lending themselves to MEM fabrication, such as the SiDRG, local variations in etch rate produce minute, but unpredictable, asymmetries that manifest themselves as a splitting of the modal frequencies (right side of Fig. 1). Although the frequency splits are small, on the order of 0.3% or less, the absolute separation between the modal frequencies coupled with their high quality factors (Q) conspire to eliminate the mechanical gain advantage that was a primary objective of sensor's design.

In past work, the resonant frequencies of the SiDRG were tuned by applying electrostatic forces with dedicated electrodes, thereby locally altering the resonator stiffness [4], [5], [6]. The drawback of this solution, however, is that the electrodes are required to maintain a voltage stability that is difficult to achieve with compact, low-cost electronics. The possibility of tuning the modes by permanently altering the mass distribution of the resonant structure is attractive because it eliminates the need for the electrostatic tuning electronics.

Though no analytical results exist regarding the effects of mass perturbations to the SiDRG's specific structure, results have been documented for a simple ring, which has similar modal characteristics. On a symmetrical ring, the $n=2$ Coriolis-coupled mode¹ is planar with an elliptical shape and can occur with any pair of orthogonal diameters (left hand side of Fig. 2). Studies of slightly asymmetric rings show that the rings have approximately the same elliptical mode shape for the $n=2$ Coriolis-coupled mode, but the mode shape only occurs in two fixed orientations, forty-five degrees apart, and at two nearly degenerate modal frequencies (right hand side of Fig. 2) [8], [9]. Equations have been derived concerning the effects of mass perturbations on the positions of the modal axes and their modal frequencies and these results have been verified on physical systems [8], [7]. These equations were then used to derive a remarkably simple frequency tuning method in which a point mass is added to the location of the anti-node of the high frequency mode or removed from the location of the anti-node of the low frequency mode to remove the frequency split [9]. Later, laser ablation was performed on a MEM rings to remove mass and predictably alter the frequency split [10], [11]. Unfortunately, determining the location of the anti-nodes requires significant laboratory effort and does not lend itself to a production environment. The objective of this paper is to develop a tuning algorithm that will use experiments performed by the embedded electrodes as its solitary guide.

In order to facilitate the development of the methodology, a scale model of the SiDRG, named the Macro

¹We will focus on $n=2$ Coriolis-coupled mode because it is the mode most commonly used to operate similar structures as a rate-sensing gyroscope. Much of the analysis applies to higher-order Coriolis-coupled modes as well but has been ignored here for simplicity.

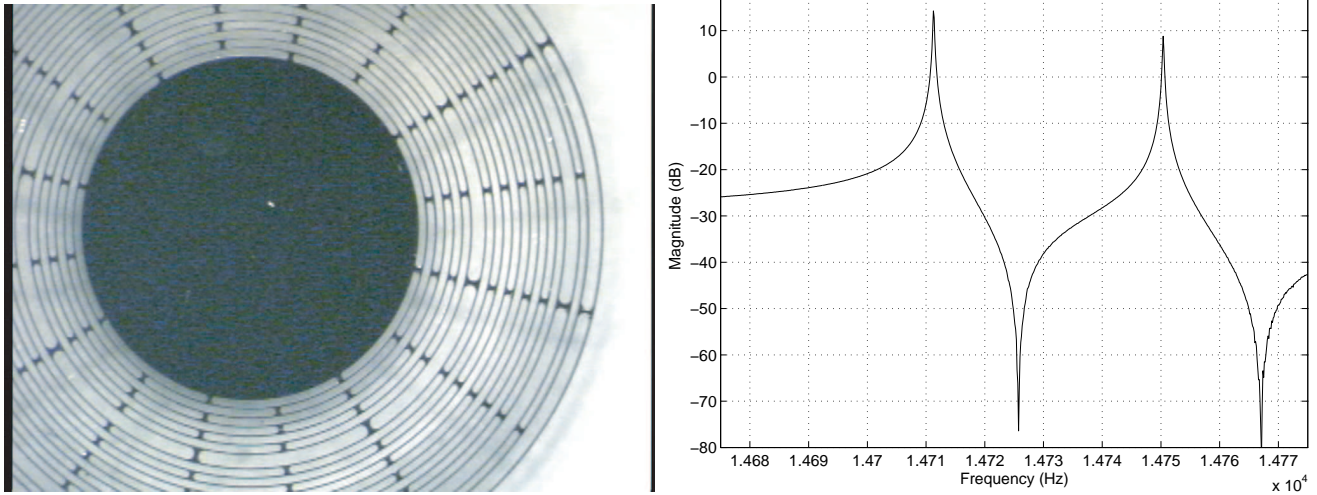


Fig. 1. **Left:** Photograph of an unpackaged Boeing Silicon Disk Resonator Gyroscope (SiDRG). In the packaged device, electrodes are placed in spaces between the rings to control and sense planar vibrations. The $n=2$ Coriolis-coupled mode of the resonator is generally utilized for rate detection. **Right:** SiDRG frequency response using embedded drive and sense electrodes within a narrow, 100 Hz band encompassing the “fundamental” Coriolis modes. Though the frequency split is small in a relative sense –less than 0.3% –the sensor effectively has no mechanical gain in this state. The present work proposes a systematic method for tuning these modal frequencies to degeneracy by making small perturbations to the resonator’s mass distribution.

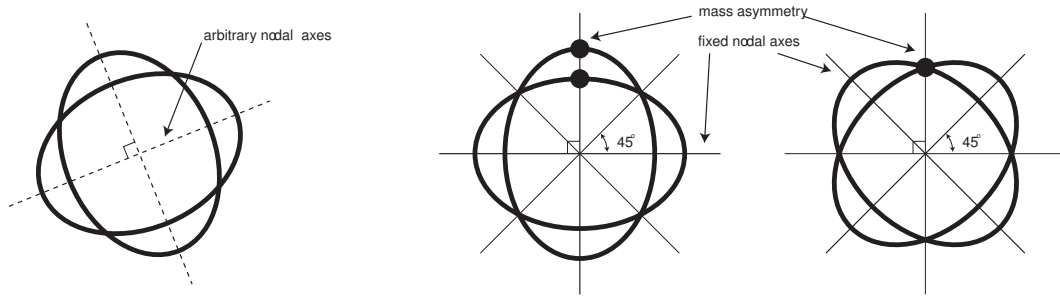


Fig. 2. **Left:** The mode shape of the “fundamental” Coriolis mode in a symmetric ring is ellipsoidal. The mode can exist with any pair of orthogonal nodal axes. **Right:** When a slight mass asymmetry exists the mode only occurs in two orientations, forty-five degrees apart. These modes have two slightly different frequencies and represent a detuning as seen in Fig. 1. **Should they be call anti-nodal axes? or should all my axes be rotated 45 degrees?**

DRG, was fabricated for this study (Fig. 3). A novel model identification method is developed and tested using empirical frequency responses from the drive and sense pickoffs. Mass perturbations of the Macro DRG are done using small magnets and are modeled as perturbations to the mass matrix identified in the model. The prospect of achieving a tuned state by placing magnets in only one angular location on the resonator is analyzed at depth before a more elegant frequency tuning approach is revealed. This approach uses only the fixed electromagnetic actuators and fixed capacitive sensors to guide the process, successfully removing the need to directly identify the location of anti-node of the high frequency mode. In the last section, this approach is successfully demonstrated under several different initial conditions.

B. MACRO DRG EXPERIMENTAL SETUP

The Macro DRG resonator is a magnetized steel simulacrum of the SiDRG resonator with an outer diameter of 12 cm (Fig. 3). Each of its nineteen rings has a thickness of 1 mm, is spaced from the other rings by 1 mm, and has a thickness of 4mm. Each ring is connected its immediate neighbors at eight “spokes,” forty-five degrees apart. The positions of the eight “spokes” alternate between rings between positions 22.5 degrees from each other, as shown. Thus the structure has sixteen “spoke” locations. Small NdFeB magnets, disc shape with a 1.4 mm diameter and 0.75 mm thickness, are placed on the top surface of the resonator to create reversible mass perturbations.

Actuation and sensing of the resonator are achieved using electromagnetic actuators ² and capacitive sensing pick-offs, each shown in Fig. 3. The electromagnets are a modified relays, using variable current through its solenoid to exert a radial force on the resonator. The sensing pick-off consists of a brass disk (5mm diameter) placed parallel to the outside edge of the outermost ring of the resonator. The resonator is biased at 50 Volts so that the capacitance between the resonator and the brass disk oscillates as the resonator vibrates. The oscillation causes current to flow to the virtual ground of the transresistance amplifier. The $1M\Omega$ resistor in the amplifier circuit provides a gain of $10^6V/A$ so that the signal output will be at an observable level for the DSP. The transresistance electronics are enclosed in a steel shell to provide suitable magnetic shielding. *Finally, a thin sheet of brass surrounds the transresistance amplifier electronics to provide electronic shielding.***ASK M**

The entire experimental apparatus is shown in Fig. ???. Two electromagnets are placed forty-five degrees so that they present “orthogonal” excitations with respect to the $n=2$ Coriolis-coupled modes. The two sensors are placed forty-five degrees so that they can best sense these modes.

The block diagram for open loop system identification is shown in Fig. 4. A DSP generates band-limited signals in the range where the frequency response is desired. Since the electromagnet always causes an attractive force, the desired AC waveform is biased by 3 volts to create a strictly positive op-amp driving output. The sense signals are then further amplified four hundred times, filtered with eight pole butterworth filters possessing 10kHz cut-off frequencies, and then sampled by the DSP. The drive signal is subjected to the same filter and resampled to account for the phase shift from the filter.

The frequency response magnitude is effected by the gaps between the outermost ring of the resonator and the capacitive sensors in such a way that calibration is required. With this in mind, the actuators and sensor are

²Electromagnetic actuation is used in the Macro DRG instead of electrostatic actuation because electrostatic forces are too weak for effective activation at the Macro DRG scale. Furthermore the small gaps that are required for electrostatic actuation create a large amount of nonlinear squeeze film damping.

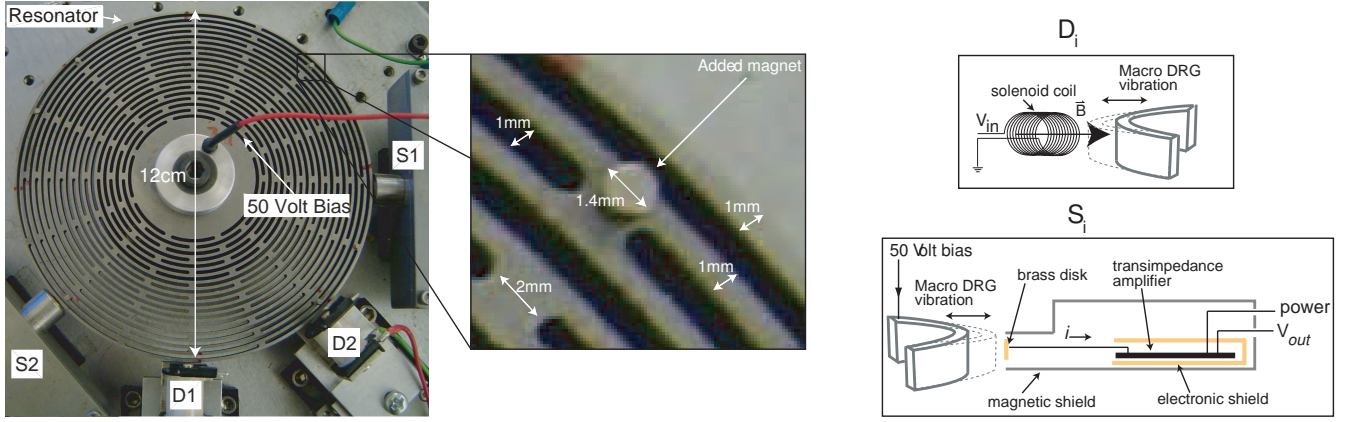


Fig. 3. **Left:** Photograph of the Macro DRG with some relevant dimensions. The two electromagnetic actuators are labeled D_1 and D_2 , and the two capacitive pick-offs that detect planar deflection of the resonator are labeled S_1 and S_2 . The small NdFeB magnet is added to create a reversible perturbation to the mass of the resonator. **Right/Top:** Diagram of the electromagnetic actuator. **Right/Bottom:** Diagram of the capacitive sense pick-off. This design was used to minimize electromagnetic coupling to the sensor.

placed on linear translational stages for precise gap control. The calibration setup for the sensors is shown as the dotted lines in Fig. 4. First, the inputs to the electromagnet are set to zero volts and the 50V bias to the resonator is replaced by a 1.6 KHz sine wave from a signal generator. The responses from the pick-offs are compared to each other and the gaps of each of the pick-offs are adjusted until the responses exhibit the same amplitude. This process ensures that the pick-offs will have the same gain at frequencies near that of the fundamental Coriolis-coupled modes. The electromagnets are much harder to calibrate, but the same level of precision is not required due to the nature of the force created by the magnetic flux. The gap is set to 1mm, which is large enough to have a minimal detrimental effect on the quality factor of the resonator while still achieving an adequate signal to noise ratio.

A single channel of Macro DRG frequency response data is shown in Fig. 5. The fundamental Coriolis modes are near 1.6kHz and appear as one resonant peak at this scale. The zoomed frequency responses, shown at the right, display the individual Coriolis-coupled modes with approximately a 2 Hz (0.12%) frequency split. This two-input/two-output empirical frequency response test will be used as the principal guide to the model fitting and tuning algorithms.

C. SENSOR MODEL

I. Model Development

The system identification method used to guide the mass perturbation process is based on the one developed by the authors for electrostatic tuning of the gyro dynamics [6]. For mass tuning, the linear mechanics of nearly

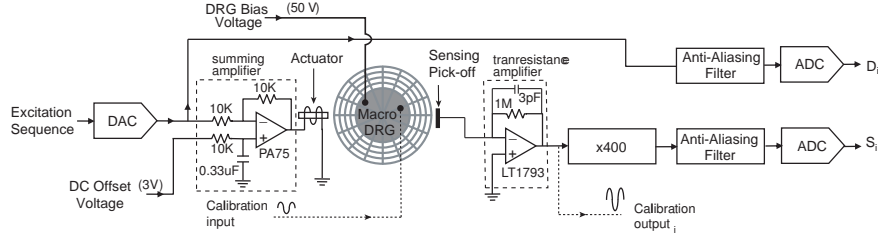


Fig. 4. Block diagram of test setup. Filtered drive and sense signals are denoted D_i and S_i , $i = 1, 2$. Frequency response data is used to construct a two-input/two-output model of the sensor. The method for for calibrating the capacitive sensors is shown as the dotted path.

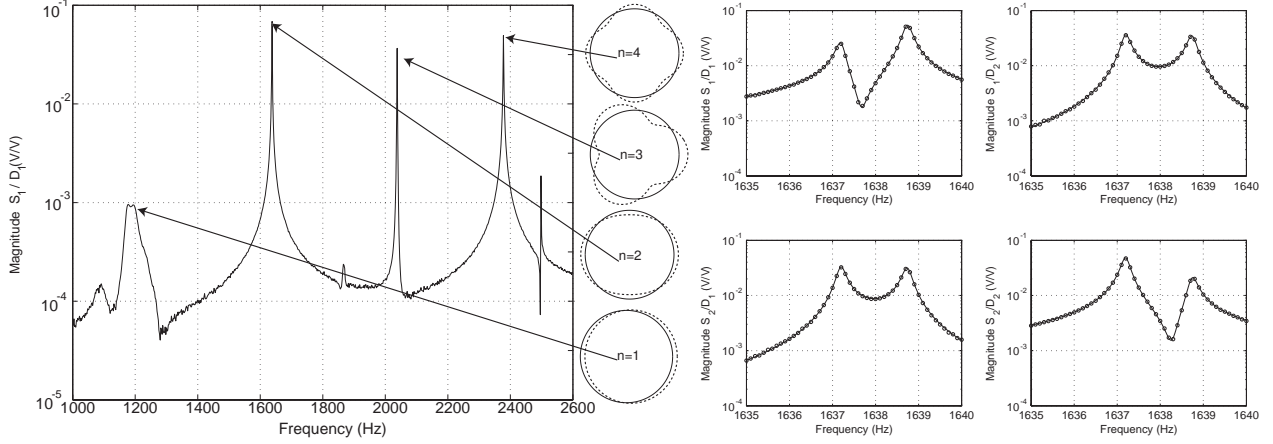


Fig. 5. **Left:** The S_1/D_1 channel of the empirical wideband frequency response of the Macro DRG showing several modes of the resonator. At this scale there appears to be no split at the $n=2$ mode. **Right:** The narrowband dynamics of all four channels in a neighborhood of the fundamental Coriolis-coupled modes. ‘o’ is used to represent the data while the line through the points is a fit using the modelling process described later in this paper. Just as in the SiDRG response, the Coriolis-coupled modes of the Macro DRG have a small but detrimental frequency split despite the fact that the steel resonator visually exhibits symmetry.

degenerate vibratory gyros in a neighborhood of the Coriolis-coupled modes can be modeled as

$$H_{out}(s)RZ_{act}^{-1}(s), \quad (1)$$

where s is the Laplace transform variable and where

$$Z_{act}(s) := (M_0 + \Delta_k)s^2 + Cs + K. \quad (2)$$

In this model C , and K are real 2×2 positive definite damping and stiffness matrices, respectively. M_0 is the real 2×2 positive definite nominal mass matrix and Δ_k is the perturbation to the mass matrix due to the particular arrangement of added magnets in the k th perturbation case. The angular rotation rate of the sensor is assumed to be zero in this model. The subscript on Z_{act} denotes that the system matrices are written in the generalized coordinates specified by the actuator (forcer) frame. The transfer function H_{out} represents any dynamics associated with the signal conditioning electronics and $R \in \mathbf{R}^{2 \times 2}$ captures the effects of noncolocated pick-offs and forcers.

The model parameters $\{C, K, M_0, \Delta_1, \Delta_2, \dots, \Delta_{n_p}, H_{out}R\}$ are estimated by using frequency response data from $n_p + 1$ experiments conducted with different mass perturbation scenarios. In other words, the k th experiment yields two-input/two-output complex-valued frequency response data $\{\psi_{k,1}, \psi_{k,2}, \dots, \psi_{k,m_k}\}$, $\psi_{k,j} \in \mathbf{C}^{2 \times 2}$, corresponding to the m_k real frequencies $\{\omega_{k,1}, \omega_{k,2}, \dots, \omega_{k,m_k}\}$.

The minimax optimization problem for estimating the sensor parameters is

$$\min_{\substack{M_0 + \Delta_p > 0 \\ K > 0, C > 0, M_0 > I \\ R_l \in \mathbf{C}^{2 \times 2}, l = 0, 1, \dots, n_R}} \max_{\substack{k=0, \dots, n_{exp} \\ q=1, \dots, m_k}} \bar{\sigma}(\tilde{R}_{k,q} - \psi_{k,q} Z_{act}(j\omega_{k,q})), \quad (3)$$

where

$$\tilde{R}_{k,q} := \sum_{l=0}^{n_R} R_l \omega_{k,q}^l, \quad (4)$$

and where evaluating Z_{act} at the q th frequency point associated with the k th experiment yields

$$Z_{act}(j\omega_{k,q}) := -(M_0 + \Delta_k) \omega_{k,q}^2 + K + jC\omega_{k,q}. \quad (5)$$

The $M_0 > I$ constraint in (3) is imposed rather than the typical $M_0 > 0$ because in the latter case all of the free parameters may scaled by a nonzero constant so as to make the cost arbitrarily small without actually changing the model frequency response. Also note that $H_{out}R$ has been replaced by \tilde{R} . This recognizes the fact that any additional dynamics due to, for example, signal conditioning preamplifiers, should not exhibit significant magnitude and phase changes in a neighborhood of the resonant modes. If these dynamics can be reflected to the sensor output then they can be combined with R into a low order polynomial function of frequency with coefficients in $\mathbf{C}^{2 \times 2}$, i.e. \tilde{R} is degree n_R . In fact, \tilde{R} can be viewed as combining the first few terms of the Taylor series expansion of the frequency response function of H_{out} including the non-collocation effects.

Finally $\bar{\sigma}$ denotes the largest singular value. Thus, in (3), $\bar{\sigma}(\tilde{R}_{k,q} - \psi_{k,q} Z_{act}(j\omega_{k,q}))$ can be viewed as a nonconventional norm of the estimation error at each data point. The minimax optimization problem will choose model parameters to minimize the maximum value of this norm over the frequency set chosen. Note that this form of the optimization has the advantage that it can be restated as the linear matrix inequality given by

$$\begin{aligned} \min: & \quad \gamma \\ \text{subject to:} & \quad J_{qk} > 0, q = 1, \dots, m, k = 0, \dots, n_p \\ & \quad M_0 > I, (M_0 + \Delta_k) > \mathbf{0}, C > \mathbf{0}, K > \mathbf{0} \\ & \quad \Delta_0 = 0, R_l \in \mathbf{C}^{2 \times 2}, l = 0, \dots, n_R \end{aligned}, \quad (6)$$

where

$$J_{qk} := \begin{bmatrix} \gamma I & (\tilde{R}_q - \Psi_{k,q} Z_{\text{act}(k)}(j\omega_q))^* \\ \tilde{R}_q - \Psi_{k,q} Z_{\text{act}(k)}(j\omega_q) & \gamma I \end{bmatrix}$$

which can be efficiently solved using a number of commercially available packages.

II. Model Verification

Experimental data is generated by driving each actuator with a narrow band chirp sequence that encompasses the Coriolis modes of the Macro DRG. The input-output sequences are processed to yield 2×2 empirical frequency response data on a grid of frequencies with 0.1 Hz resolution. The model (2) is applied to two mass perturbation cases in addition to the nominal case when no mass perturbation is present. The first mass perturbation case places four magnets on outer ring of the Macro DRG as shown in the left-hand picture of Fig. 6 and will be represented by Δ_1 . The four-fold symmetry of the mode shape guarantees that this perturbation will have the same effect as adding the four masses to only one of these four positions. The second mass perturbation case places four magnets on the outer ring of the DRG as shown in the right-hand picture of Fig. 6 and will be represented by Δ_2 . The empirical frequency responses for these perturbed cases along with the unperturbed case (no magnets added) are shown as the plots in Figs. 7 and 8. Since the sensor is a two-input/two-output plant, four frequency response magnitude plots are shown in Fig. 7 and four frequency response phase plots are shown in Fig. 8 (the individual channels are denoted $S_1/D_1, S_2/D_1$, etc.). It is clear that mass perturbations shift both modal frequencies, change their frequency split, and also modifying their coupling. The model parameter set $\{M_0, \Delta_1, \Delta_2, C, K, R_0, R_1, \dots, R_{n_R}\}$ is determined using (6) and the three sets of frequency response data are generated for comparison with the data. The model frequency responses are given by $\Psi_{k,i} = (\sum_{l=0}^{n_R} R_l \omega_i^l) (-(M_0 + \Delta_k) \omega_i^2 + K + jC\omega_i)^{-1}$, $k = 0, 1, 2$. The order of \tilde{R} , n_R , is set to 2 for this and future models. Fifty one frequency response points are used to cover the 5Hz width around the peaks with a 0.1 Hz resolution. The model frequency responses are plotted as the solid lines in Figs. 7 and 8. The model fit is almost indistinguishable from the data and at each point is within 5%.

Since we are interested in using this model to guide the mass addition/removal process with the objective of driving the two modal frequencies together, its predictive power is of great importance and is tested in two ways. In the first test, two magnets are added to each of the four points on the resonator corresponding to the positions shown the left-hand picture in Fig. 6 (total of eight magnets). This perturbation doubles the magnitude of the mass perturbation corresponding to Δ_1 so we compare the empirical data with the frequency response of the model

$$(R_0 + j\omega R_1) (-(M_0 + 2\Delta_1) \omega^2 + K + j\omega C)^{-1}.$$

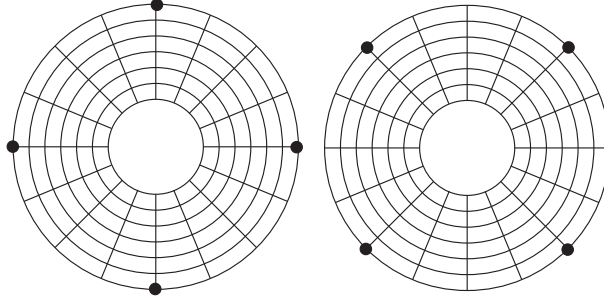


Fig. 6. **Left:** Location of Δ_1 perturbation. **Right:** Location of Δ_2 perturbation. Masses are added at four points in each case to achieve the most even possible mass loading. These are the perturbations corresponding to ‘□’ and ‘diamondsuit’ in Figs. 7 and 8.

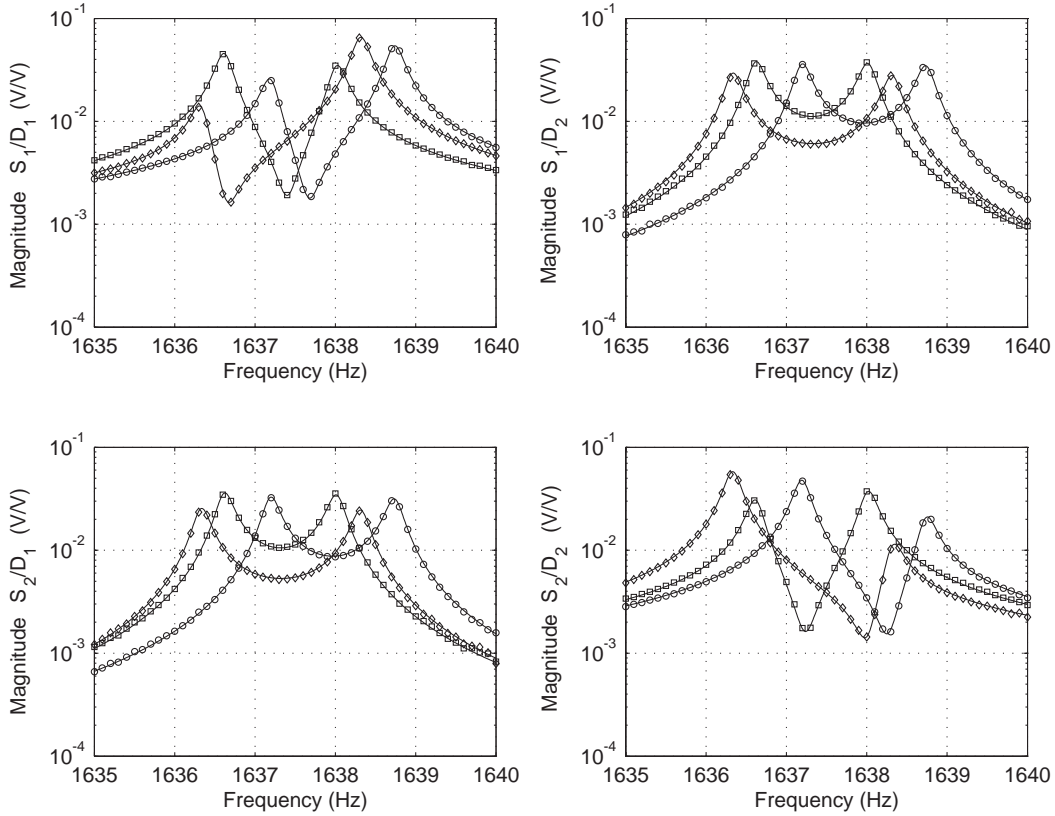


Fig. 7. The two-input/two-output empirical and model frequency response amplitudes found in the model verification experiment. The empirical data for the test with no perturbation is represented by ‘○’ and the Δ_1 and Δ_2 perturbations (shown in Fig. 6) are represented by ‘□’ and ‘◇’ respectively. The model fits given by $(R_0 + j\omega R_1)(- (M_0 + \Delta_k)\omega^2 + K + j\omega C)^{-1}$ of the three data sets are the solid traces. Thus the change in the frequency response due to the addition of magnets is successfully modeled as a change to only the mass matrix.

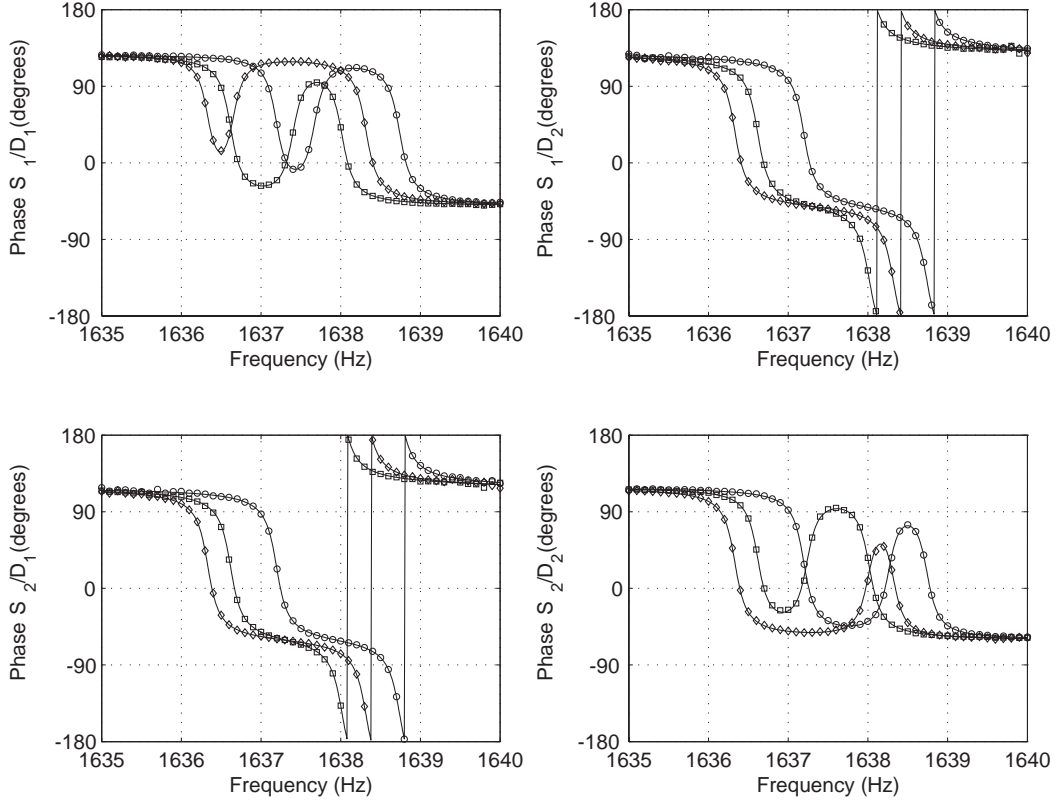


Fig. 8. The two-input/two-output empirical and model frequency response phases corresponding to the amplitudes in Fig. 7.

The comparison is made in Fig. 9. The model predicts the actual frequency response extremely well.

The second test case involves placing a single magnet at each of the eight points on the resonator corresponding to the locations shown in both pictures in Fig. 6. This perturbation should correspond to modifying the nominal mass matrix by the sum of Δ_1 and Δ_2 . Thus we compare the frequency response data against the model

$$(R_0 + j\omega R_1) \left(-(M_0 + \Delta_1 + \Delta_2)\omega^2 + K + j\omega C \right)^{-1}.$$

Again, the set of plots in Fig. 10 shows very good agreement between the model prediction and the empirical frequency response data. This verifies the predictive power of the model fitting technique and the assumption that the addition of the magnets can be modelled purely as a mass matrix perturbation.

D. TUNING THE MODAL FREQUENCIES

I. Frequency Tuning by Perturbing One Unique Angular Location

Now that the experimental setup and modelling techniques are identified, we begin to develop potential processes for driving the modal frequencies of the Macro DRG together and reaching a ‘tuned’ state. By observing Fig. 7 it is clear that the angular location of the a mass perturbation effects the resulting frequency split. For

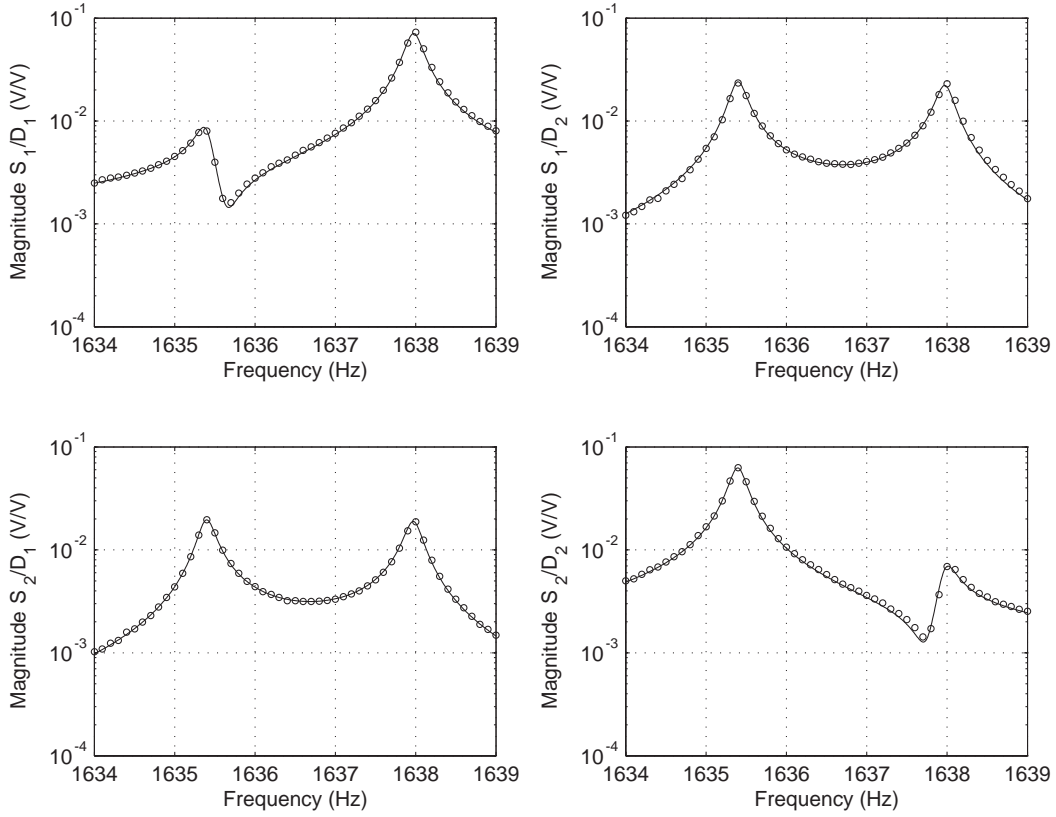


Fig. 9. Empirical frequency response of macro DRG with double the mass perturbation at the Δ_1 perturbation locations ('o') compared to the frequency response predicted by the model $\tilde{R}(j\omega)(-M_0 + 2\Delta_1)\omega^2 + K + j\omega C)^{-1}$ (solid trace).

a simple ring, frequency tuning can be achieved by adding mass to only one location, which happens to be the anti-node of the high frequency mode [9]. This appears to be, in a sense, the simplest solution to the frequency tuning problem and in this section we attempt a deep analysis of this methodology. First the high frequency mode shape is mapped out using a laser vibrometer. Then, using this as a guide, single location frequency tuning is attempted in a region near the anti-node and it is confirmed that the mode shape is, indeed, a good tuning guide. Finally, two additional methods are tested that use the model fitting techniques derived in this paper to identify this ideal tuning location. These satisfy the goal of using only the electromagnetic drivers and capacitive sensors to guide the tuning process.

1) *Measuring the Mode Shape:* In this experiment, the radial motion is measured at the outer ring by a laser vibrometer. One of the electromagnets is used to excite the Macro DRG at the higher of the two $n=2$ Coriolis-coupled frequencies. The previous testing setup is placed on a rotational stage while the laser vibrometer is in fixed position (Fig. 11). Vibration measurements were taken every two degrees on a 90 degree arc. The resulting mode shape is shown as the right hand plot of Fig. 11, with the peak displacement occurring at 77 degrees. It is important to note that the mode shape follows a sine wave fairly well, but not perfectly. This is essentially

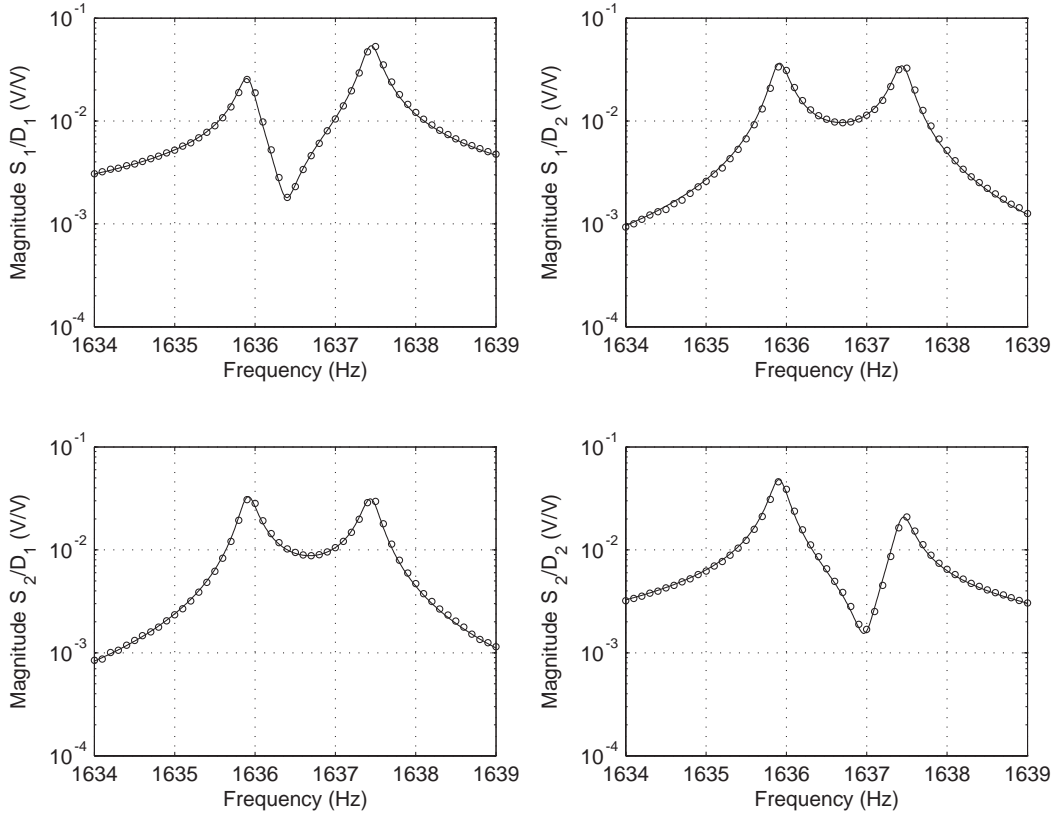


Fig. 10. Empirical frequency response of macro DRG with the mass perturbations in both the Δ_1 and Δ_2 perturbation locations ('o') compared to the frequency response predicted by the model $\tilde{R}(j\omega)(-(M_0 + \Delta_1 + \Delta_2)\omega^2 + K + j\omega C)^{-1}$ (solid trace).

the procedure for identifying a mass tuning location suggested for simple rings and provides some interesting information, but does not satisfy the stated goal of using only the fixed electromagnetic drivers and capacitive sensors to guide the tuning.

2) *Testing Frequency Tuning Near the Anti-node:* We first attempt to tune by repeatedly placing magnets at 76 degrees from the D_1 axes and measuring the empirical frequency responses between magnet additions. The resonant frequencies from these responses are calculated by taking the square roots of $\lambda_{M,K}^{high}$ and $\lambda_{M,K}^{low}$, the larger and smaller eigenvalues of the modeled mass and stiffness matrices as derived from the empirical frequency responses. The split (difference) between these frequencies is plotted in the right hand plot of Fig. 12. At first the split decreases, but, after a certain point, the additional magnets increase the split. This practice was repeated at 72, 74, 78 and 80 degrees from the D_1 axes and the data is plotted in Fig. 12. Though the plots are crudely faceted due to discrete amount of mass added with each magnet, it still appears from Fig. 12 that the best tuning location is approximately 77 degrees from the D_1 axes. It should be noted, however, that by misplacing magnets by only 3 degrees, the minimum achievable split is increased from about 0.15 Hz to 0.4 Hz. This behavior follows what is predicted using the equations in [9] for a simple ring and is fairly simple to explain. When mass is placed

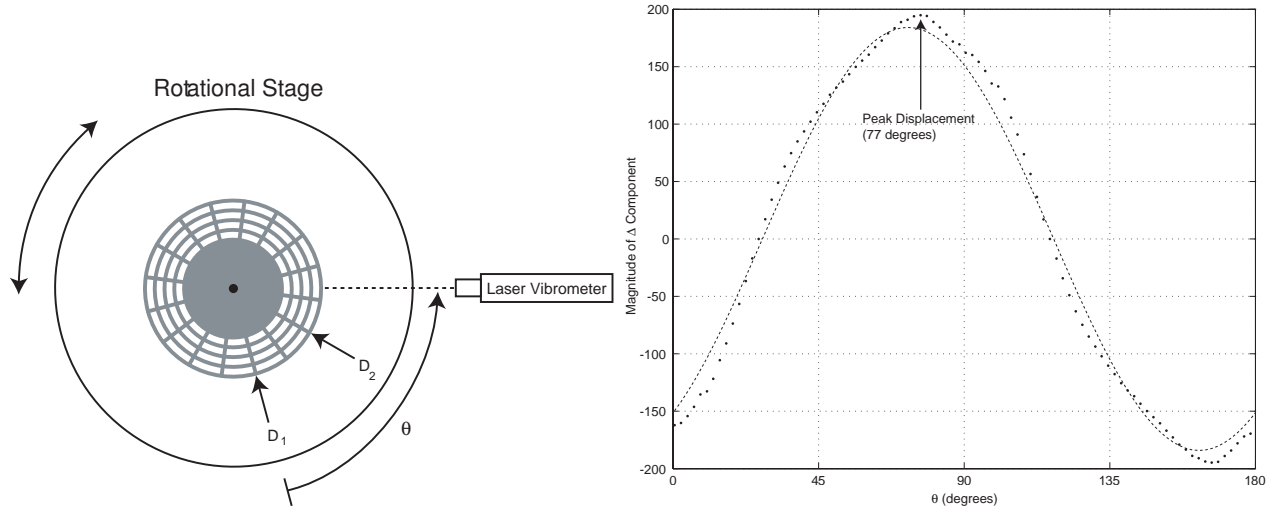


Fig. 11. **Left:** Illustration of the testing setup used to determine the radial deflection of the outermost ring of the Macro DRG resonator. The driving electromagnet and the resonator are fixed on the rotational stage, so that the deflection can be measured at very fine increments. **Right:** Plot of the radial deflection as a function of angular position. The dots represent the experimental data, while the dotted line is closest sine wave fit (**not sure the best way to say this...i used an fit of the data and used only the first harmonic to make the plot**). The larger deviations from the sine wave are most likely caused by the additional stiffness provided by the spokes. Also, the dynamics of the system subtly changed throughout the experiment, causing a couple small irregularities to the plot. One proposed tuning method involves adding mass directly to the resonator at the location corresponding to the anti-node of the experimental data. This is the method that has been used in the past to tune other ring shaped devices. Our goal is to develop a process that would only use the fixed electromagnetic actuators and capacitive sensors.

directly at the locale of the high frequency mode, the frequency split is reduced, and the anti-node remains in the same location. If more mass is added after the split reaches zero, the locale where mass is added becomes the new low frequency anti-node and the split begins to increase. If the initial magnet is misplaced, however, the high frequency anti-node shifts away from the locale of the added magnet. The split then begins increase when the added magnet is closer to the low frequency anti-node. Thus, as the error in the location choice increases, the frequency split begins to increase with fewer added magnets and minimum achievable split increases.

The solid line on the right hand side of Fig. 12 is an attempt to simulate the minimum achievable split if mass could be added in smaller amounts when tuning 76 degrees from the D_1 axes. The Δ associated with the first four magnets added was found using a model fit to the empiricial frequency response data of the unperturbed case and the case with four magnets added at 76 degrees. The solid trace on the plot is the predicted split using this Δ , ie. the difference in the frequencies derived from $\lambda_{M_0 + \frac{\alpha}{4}\Delta, K}^{high}$ and $\lambda_{M_0 + \frac{\alpha}{4}\Delta, K}^{low}$ where α is the number magnets added. Thus it is clear that the model fitting process would prove helpful in determining the minimal split associated with a particular mass perturbation. This inspires the first proposed tuning method.

3) Δ as a Function of Angular Position on the Outer Ring: A function $\bar{\Delta}(\theta)$ is defined as the relationship between $\bar{\Delta}$, the mass matrix perturbation associated with the one magnet placed upon the outermost ring, and θ ,

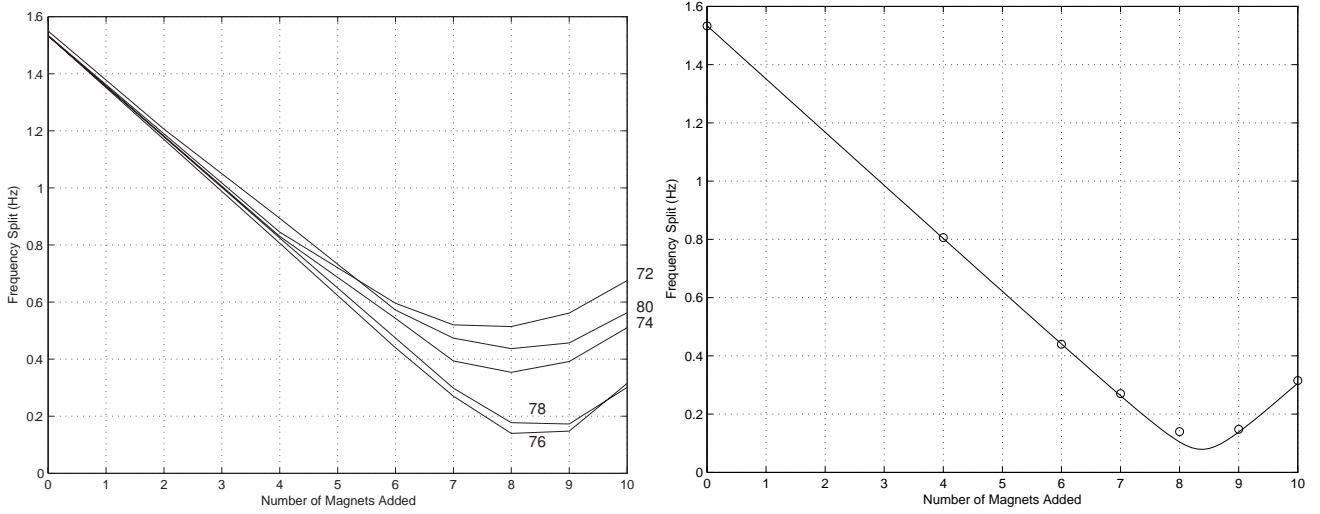


Fig. 12. The five traces on the left hand plot represent five experimental attempts to tune the Macro DRG by placing magnets at only one angular location, using locations of 72, 74, 76, 78 and 80 degrees. Data was taken when 0,4,6,7,8,9 and 10 magnets were added for each case. The frequency splits were found by taking a two by two frequency response at each of these points, fitting a model to the data, and using the generalized eigenvalues of the modeled M and K matrices. In each case the split is at first reduced but begins to increase before becoming less than $0.1Hz$. It appears that the smallest split would be achieved using near a location near 77 degrees. It is interesting to note that if the placement is as much as 3 degrees away from this location, the minimum split increases to $0.4 Hz$. The plot at right shows only the data taken for at 76 degrees. The solid line fit is done by fitting the empirical data from the first two points to a set $\{M_0, \Delta, C, K, R_0, R_1\}$ and using $\lambda_{M_0 + \frac{\alpha}{2}\Delta, K}^{high}$ and $\lambda_{M_0 + \frac{\alpha}{2}\Delta, K}^{low}$ to determine the split (where α is the number of masses added). This is a good test of the predictive relevance of the model, but also shows the minimum achievable split if mass could be added in fractions of a magnet.

the angular position of that additional magnet. Once the function $\bar{\Delta}(\theta)$ is known, an angle, θ , and a scalar number of magnets, α , can be found such that $\lambda_{M_0 + \alpha\bar{\Delta}(\theta), K}^{high} = \lambda_{M_0 + \alpha\bar{\Delta}(\theta), K}^{low}$. An experiment is performed to find $\bar{\Delta}(\theta)$ for values of θ in one ninety degree arc³. Eight separate perturbations were conducted with magnets spaced in 11.25 degree steps (a total of nine MIMO frequency response data sets) and then the model parameter set $\{M_0, \Delta_1, \dots, \Delta_8, C, K, R_0, R_1\}$ was identified. Plots of the upper diagonal, lower diagonal and off diagonal terms of each Δ_k , $k = 1, 2, \dots, 8$, are shown in Fig. 13. By linearly interpolation, $\bar{\Delta}$ can be approximated for any θ . When $\theta = 75.4$ degrees and $\alpha = 8.4$ magnets, $\lambda_{M_0 + \alpha\bar{\Delta}(\theta), K}^{high}$ and $\lambda_{M_0 + \alpha\bar{\Delta}(\theta), K}^{low}$ are equal making the system tuned. If we were to rely solely on this data to perform the tuning, a final split of about $0.2Hz$ would be achieved (using data from Fig. 12), which is pretty good. Unfortunately, it would not be practical to use the experimental relationship of Fig. 13 on a different Macro DRG. Any small difference in the drive and sense gap distances or the internal stiffness and damping might effect the relationship. Thus, to use this approach, this entire experiment would have to be repeated for every new device, requiring excessive and perhaps unnecessary perturbations.

³It can be shown that adding the same mass at 90 degree, or 180 degree, angles relative to the current position produces the same mass matrix perturbation for the modes of interest.

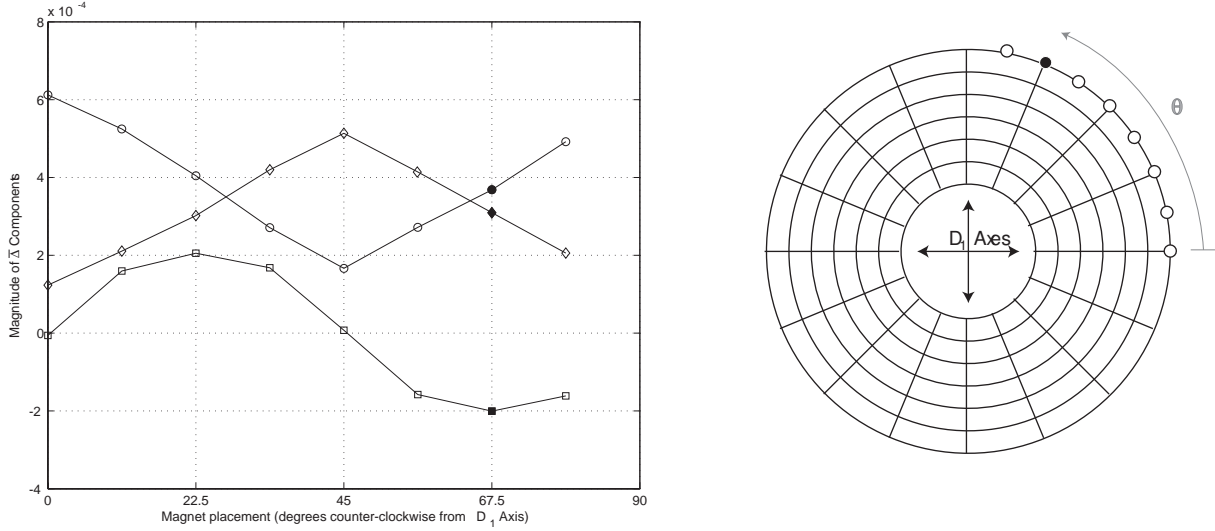


Fig. 13. **Left:** Mass matrix perturbation, $\bar{\Delta}$, as a function of the counter-clockwise angle from the D_1 axis, θ , found by fitting the model to ten empirical frequency response data sets. The upper diagonal term is denoted by ‘◇’, the lower diagonal by ‘○’, and the off diagonal term by ‘□’. **Right:** Illustration of the eight placements of the magnet in the tests. When the experiment is repeated with different lengths for the actuators and sensors, and different initial magnet distributions, the functional relationship varied only a little. The absolute magnitudes are not important because model parameter set by the $M_0 > I$ constraint. The relative magnitudes, however, are at the very least interesting. The filled in black data point and magnet is meant to illustrate the perturbation done to achieve the set of data points at 67.5 degrees.

4) *The Eigenvectors of M and K :* In the second method, the generalized eigenvector associated with the $\lambda_{M,K}^{high}$ is used to identify the location of the high-frequency anti-node. Though $\lambda_{M,K}^{high}$ is known to be the square of the higher natural frequencies of the model, the physical interpretation of the generalized eigenvectors relies on the coordinate system of the equations of motion. Because the coordinates of the generalized eigenvectors are in the drivers’ reference frame (refer to (1)), the ratio of the components of the generalized eigenvectors are the ratio of the amplitudes of the velocity of the Macro DRG at the two actuators when it is excited at its corresponding eigenfrequency. In order to use this information to estimate at the mode shape, the amplitude of the radial motion, u , is approximated by $u = A \cos(2(\theta - \Phi))$ where A is the maximum amplitude of the velocity and θ is the angular location as measured from the D_1 axis (Fig. 14). This is clearly an approximation of the true shape given in Fig. 11. The amplitude of motion at the first and second driver would be $A \cos(2\Phi)$ and $A \sin(2\Phi)$ respectively. Thus Φ , the angular location of anti-node of the high frequency mode, can then be approximated by

$$\Phi = \frac{1}{2} \tan^{-1} \left(\frac{v_1}{v_2} \right), \quad (7)$$

where v_1 and v_2 are the values of first and second term respectively of the eigenvector associated with $\lambda_{M,K}^{high}$. In the case of the unperturbed Macro DRG $\Phi = 75$ degrees. This method is particularly attractive because it does

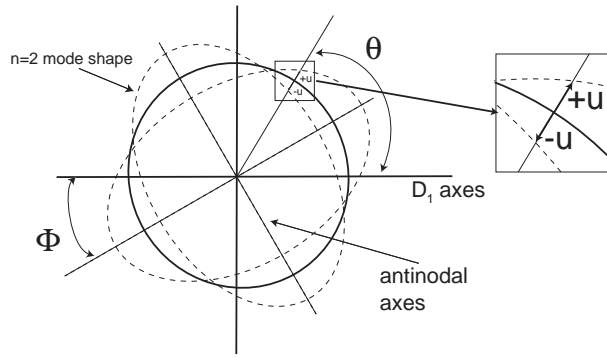


Fig. 14. Illustration of the assumed mode shape of the ring using $u = A\cos(2(\theta - \Phi))$, where Φ indicates the location of the anti-nodes of the mode shape, and u is the radial displacement of the mode shape, as a function of the angle θ . We will use this notation to approximate the mode shape of the Macro DRG.

not require any experimentation besides the initial frequency response test to approximate the location of the anti-nodes. It appears to be slightly less accurate than the estimate found directly using $\bar{\Delta}$ and would have a minimal split of approximately 0.3 Hz split.

This method can be improved if one abandons the notion of using only one angular location for tuning. In this improvement, after each magnet is added and a new empirical frequency response is performed, a new model parameter set is found with a new anti-node location. This new location is the target for the next added magnet. Essentially, the effect of the estimate error is negated by chasing the location of the high frequency anti-node around the ring. This method proves successful, guaranteeing a final frequency split of less than 0.1 Hz, but lacks elegance and would be difficult to practice on the SiDRG. A more elegant method is presented in the next section in which the anti-node is essentially “trapped” between two spokes on which mass is added.

Actual Ideal Locale	77 degrees
Anti-node Location (using vibrometer)	77 degrees
$\bar{\Delta}(\theta)$ prediction	75.4 degrees
Eigenvector prediction	75 degrees

II. Tuning Using the Spokes

When the tuning problem is generalized to allow two tuning locations, the solution is much more robust to errors in placement. By choosing mass loading locations on either side of the anti-node of the high frequency mode, the anti-nodal orientation is, in a sense, trapped. For a MEMs structure such as the SiDRG, it will be easiest to add mass at the “spokes” of the resonator (visible in Fig. 3) as the structures that join adjacent rings and

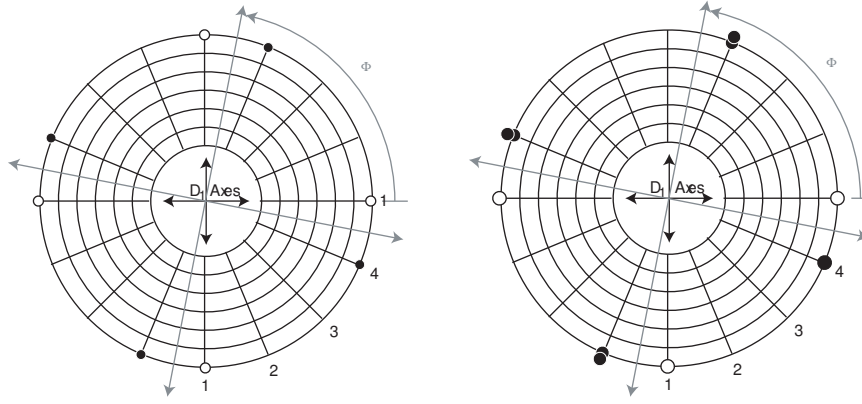


Fig. 15. **Left.** Illustration of the identified spokes for mass loading for the example in the text. The gray axes represent the approximated anti-nodal axes of the unperturbed Macro DRG. The small white circles represent where the two magnets may be placed to calibrate the spoke 1, and the two black circles represent where two more may be added to calibrate the spoke 4. **Right.** The final orientation of the magnets that successfully tunes the Macro DRG so that the anti-nodal axes are “trapped” between the tuning spokes. The calibrations in the previous steps are used to choose this orientation.

form a radial pattern) that are closest to the anti-node. In this scenario the perturbed mass matrix is given by

$$M = M_0 + \alpha_1 \Delta_1 + \alpha_2 \Delta_2, \quad (8)$$

where Δ_1 and Δ_2 correspond to the mass matrix perturbations associated with the addition of mass to the two tuning spokes.

This process can be described as a three step algorithm. As an example, we start with the data for the unperturbed Macro DRG (represented by ‘o’ in Fig. 16). In the first step, a model is fit to this data set and Φ is approximated as 79 degrees using (7). This location is between the spokes labelled 4 and 1, thus these are chosen as the locations for tuning. The second step acts as a calibration step for the mass matrix perturbations Δ_1 and Δ_2 . Two magnets are added to spoke 4 to represent the Δ_1 perturbation and an empirical frequency response is measured. Then, two magnets are added to spoke 1 and a third frequency response is measured. Using the three frequency response sets, the model parameters $\{M_0, \Delta_1, \Delta_2, C, K, R_0, R_1\}$ can be found. Fig. 16 shows the three empirical frequency of the first two steps. As expected, with each added magnet the resonant frequencies and their relative split are reduced. In the third step the numbers of magnets that need to be added to each spoke are calculated. This problem is solved with $\alpha_1 = 7.2$ and $\alpha_2 = 3.2$, rendering the system with M as in (8) degenerate. We can only add quantized amounts of mass onto the rings, so 3 masses are added to the spoke 1, and 7 to the spoke 4. The final empirical frequency response is acquired and is shown in Fig. 17. Note that the response in the off diagonal channels is reduced, which is the expected result in a degenerate sensor. After model identification is performed on this last data set, the split is found to be only 0.08 Hz. For our purposes, the sensor is tuned.

The algorithm was then applied to an array of initial mass distributions in order to test its performances on

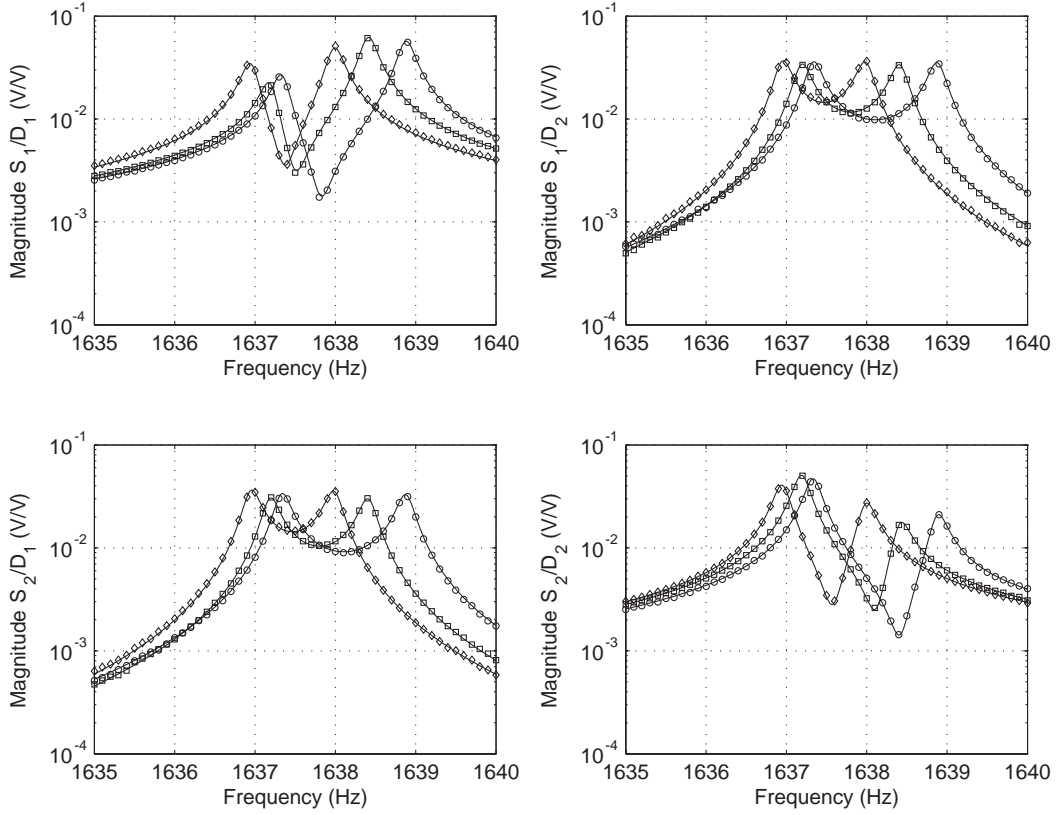


Fig. 16. Frequency responses from steps 1 and 2 of the algorithm with their corresponding fit. ‘o’ represents the empirical response from the unperturbed case, ‘□’ represents the response when magnets are added only to spoke 4 and ‘◇’ represents when magnets are added to spoke 4 and spoke 1. Again the solid lines represents the model fit performed on the the three sets. The model associated with this fit is used to determine the number of magnets needed to be added in order to achieve a tuned state. The frequency response after the tuning magnets are added can be seen in Fig. 17.

multiple cases. For these tests, a larger magnet (diameter 8mm) is placed on the outside of the ring at positions $\{0, \frac{\pi}{16}, \dots, \frac{7\pi}{2}\}$ from D_1 for the initial arrangement. A fine tuning step is added to aid the final results. If the split in the third step is more than some threshold than one additional magnet is added to the spoke closest to the approximated location of the high frequency anti-node. In this case a threshold of 0.10 Hz is chosen, because the most a single magnet can reduce a split is .20 Hz. The results are shown in the table below. In all but one case the final frequency split is below the threshold, and can be thought of as successfully tuned. It turns out that the static threshold is not the best way to determine if an additional magnet on a spoke would further reduce the split. A threshold that is dependent on Φ is actually more desirable, and could be discussed if there was more room.

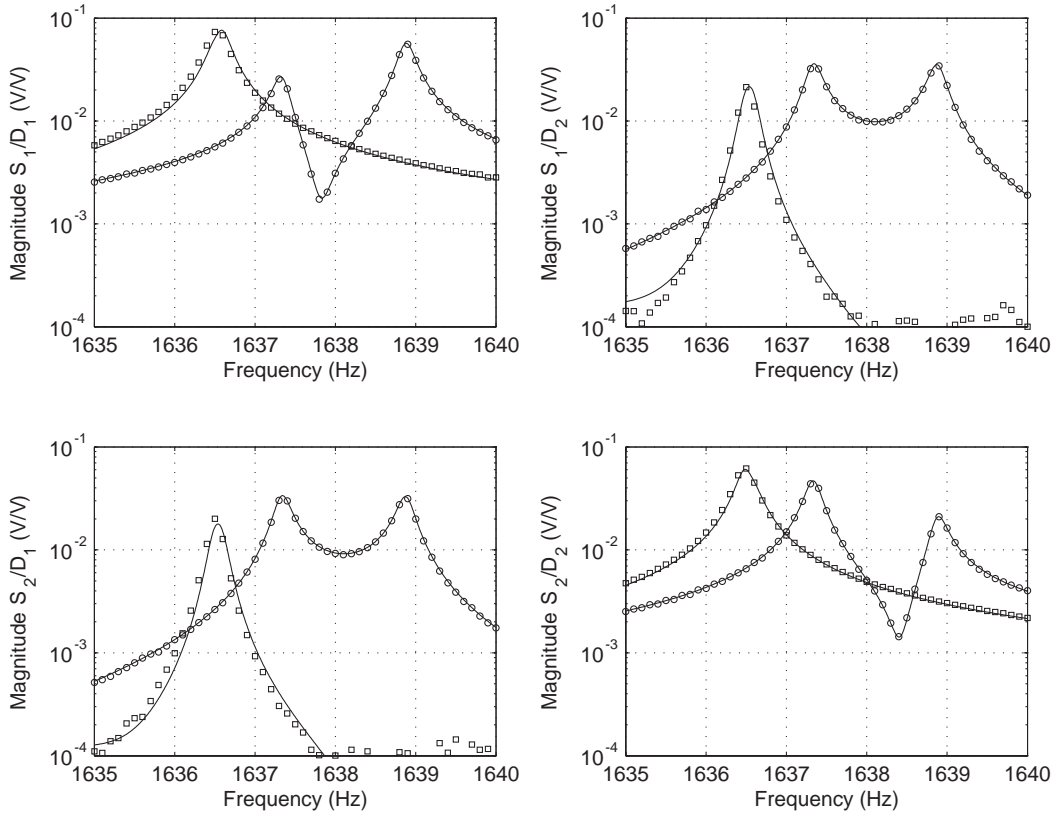


Fig. 17. The empirical frequency response of the unperturbed resonator is again represented by ‘o’. Using the model of the data in Fig. 16, weightings of 3.2 magnets on spoke 1 and 7.2 magnets on spoke 2 are predicted to give a tuned split. ‘□’ represents the empirical frequency response when 3 magnets are on spoke 1 and 7 magnets are on spoke 2. The solid line corresponding to this data is the predicted response using the model. The final split is 0.08 Hz.

Large Magnet Placement (degrees)	First Spoke	Second Spoke	Perturbation for first spoke (# of magnets)	Perturbation for second spoke (# of magnets)	Frequency split (Hz)	Iterative Spoke	Final Frequency Split (Hz)
na	1	2	7	4	0.14	4	0.08
0	2	1	6	5	0.12	2	0.08
15	1	2	4	2	0.10	4	0.08
30	1	4	6	1	0.10	1	0.10
45	1	2	9	0	0.12	4	0.12
60	1	2	11	5	0.13	4	0.08
75	1	2	8	8	0.03	na	na

E. CONCLUSIONS

A method using a mass matrix perturbation approach for tuning the two Coriolis-coupled modes in a vibratory gyroscope has been experimentally demonstrated on a scale model of the Boeing Silicon Disk Resonator Gyro. Although mass was added to the resonator for this study, the methods are readily adapted to the situation in which mass is removed. Future work will address mass matrix perturbations that can reduce the coupling of linear acceleration to the Coriolis-coupled modes. The latter objective is important for isolating the modes used for angular rate sensing from linear acceleration of the sensor case.

REFERENCES

- [1] Loper, E.J., and Lynch, D.D., "The HRG: A new low-noise inertial rotation sensor," 16th Joint Services Data Exchange for Inertial Systems, Los Angeles, CA, Nov. 1982.
- [2] Gripton, A. "The application and future development of a MEMS SiVSG for commercial and military inertial products" IEEE Position Location and Navigation Symposium, pp. 2835, April 2002.
- [3] Lynch, D.D., "Hemispherical Resonator Gyro," in Ragan, R.R. (ed.) "Inertial technology for the future," IEEE Trans. on Aerospace and Electronic Systems, AES-20, 4, pp. 414-444, 1984.
- [4] Adams, S.G., Bertsch, F.M., Shaw, K.A., and MacDonald, N.C., "Independent Tuning of Linear and Nonlinear Stiffness Coefficients," IEEE J. Microelectromechanical Systems, Vol. 7, No. 2, pp. 172-180, 1998.
- [5] Ayazi, F., and Najafi, K., "A HARPS Polysilicon Vibrating Ring Gyroscope," IEEE J. Microelectromechanical Systems, Vol. 10, No. 2, pp. 169-179, 2001.
- [6] Kim, D-J., and M'Closkey, R.T., "A systematic method for tuning the dynamics of electrostatically actuated vibratory gyros," IEEE Trans. Control System Technology, Vol. 14, No. 1, pp. 69-81, 2006.
- [7] T. Charnley and R. Perrin "Perturbation studies with a thin circular ring." *Acustica*, Vol. 28, pps, 140-146, 1973.
- [8] D. Allaei, W. Soedel and T. Y. Yang, "Natural frequencies of rings that depart from perfect axial symmetry." *Journal of Sound and Vibration*, Vol. 111, 9-27, 1986.
- [9] C. H. J. Fox . "A simple theory for the analysis and correction of frequency splitting in slightly imperfect rings" *Journal of Sound and Vibration*, Vol 142, pp 227-243, 1990
- [10] Gallacher, B. J., "Multi-modal tuning of a ring gyroscope using laser ablation" *Proc. Inst. Mech. Eng. C*, Vol. 217, pp. 557-76, 2000.
- [11] C.P. Fell, "Method for matching vibration mode frequencies on a vibrating structure" US Pat. 5739410, 1996.
- [12] Abdelmoneum, M.A, Demirci, M.M., Lin, Y-W., and Nguyen, C.T., "Location-Dependent Frequency Tuning of Vibrating Micromechanical Resonators Via Laser Trimming," 2004 IEEE Int. Ultrasonics, Ferroelectrics, and Frequency Control Symp., pp. 272-279, 2004.
- [13] Zhbanov, Yu. K., and Zhuravlev, V. F., "On the Balancing of a Hemispherical Resonator Gyro," *Mech. Solids*, Vol. 33, No. 4, pp. 213, 1998.
- [14] Enderling, S., Hedley, J., Jiang, L., Cheung, R., Zorman, C., Mehregany, M., and Walton, A., "Characterization of frequency using focused ion beam platinum deposition," *J. Micromech. Microeng.*, Vol. 7, pp. 213-219, 2007.